Research Repository UCD

Title	Dynamic crack bifurcation in PMMA
Authors(s)	Murphy, Neal, Ali, M., Ivankovic, Alojz
Publication date	2006-11
Publication information	Murphy, Neal, M. Ali, and Alojz Ivankovic. "Dynamic Crack Bifurcation in PMMA" 73, no. 16 (November, 2006).
Publisher	Elsevier
Item record/more information	http://hdl.handle.net/10197/4908
Publisher's statement	This is the author's version of a work that was accepted for publication in Engineering Fracture Mechanics. Changes resulting from the publishing process, such as peer review, editing, corrections, structural formatting, and other quality control mechanisms may not be reflected in this document. Changes may have been made to this work since it was submitted for publication. A definitive version was subsequently published in Engineering Fracture Mechanics (73, 16, (2006)) DOI: http://dx.doi/org/10.1016/j.engfracmech.2006.06.008
Publisher's version (DOI)	10.1016/j.engfracmech.2006.06.008

Dynamic Crack Bifurcation in PMMA

N. Murphy,[*] M. Ali and A. Ivankovic

School of Electrical, Electronic and Mechanical Engineering, University College Dublin, Ireland

*Corresponding author. Email address: Neal.Murphy@ucd.ie

Abstract

An investigation of the branching characteristics of small PMMA single edge notched tensile (SENT) specimens is presented. The influence of notch depth and specimen thickness was examined and it was found that branching only occurred for thicker specimens and very short notch depths. The location at which successful branching occurred was very consistent for a given notch depth. Subsequently, however, a statistical variation of branching patterns was observed.

A series of simulations was then performed to provide further insight into these tests and in particular to examine the evolution of the fracture process region ahead of the running crack. A finite volume / cohesive zone formulation was used to model micro-crack nucleation and dynamic interaction in the process zone. The cohesive strength and fracture resistance were estimated from unnotched tensile tests and the application of LEFM to the notch test data. Even though a very simple criterion was used to govern the insertion and subsequent behaviour of the cohesive surfaces in the model, many of the experimental observations were reproduced, including high frequency oscillations in crack velocity, the substantial increase in the fracture surface area due to the formation of subsurface micro-cracks, and location at which successful branching took place.

1. Introduction

Early experimental investigations by researchers such as Schardin [1], Clark and Irwin [2], and Congleton and Petch [3] led to the following observations concerning the phenomenon of crack branching. Firstly, the velocity of the crack tips after bifurcation was very similar to that of the single crack prior to the branching event. Secondly, branching appeared to occur at a constant value of stress intensity factor, K_I, rather than at a critical crack velocity. Finally, it was recognised that branching was typically preceded by the formation of small out-of-plane crack-like defects ahead of the running crack. Congleton [4] proposed a critical stress intensity factor branching criterion based on the interaction between the main crack and these 'advance' micro-cracks. Dally [5] generalized the Congleton model to relate the stress intensity factor at the point of branching to the size of the fracture process region at the tip of the main crack.

Further developing this theme, Streit and Finnie [6] suggested that the directional stability of a quasi-static crack should be influenced by the state of stress at a finite distance ahead of the crack tip in the location where the micro-cracks or voids are formed. In this case, not only the singular terms in the stress expansions, but also the remote normal stress in the crack propagation direction should be considered. The latter is known as the T-stress, and its influence on crack stability is well known [7]. This concept was applied to dynamic crack curving by Ramulu and Kobayashi [8]. In accordance with previous findings, Ramulu *et al.* [9] observed that successful branching always took place at a constant value of K_I, which was therefore cited as a

necessary condition for branching to occur. Under these conditions, multiple off-axis secondary cracks were generated and the dynamic curving criterion provided a sufficient condition for these secondary cracks to kink simultaneously. Post-branching cracks were observed to curve in all reported cases. Earlier work by Kalthoff [10] pointed out that attraction or repulsion between the two branches is controlled by the ratio K_{II}/K_I. Ramulu *et al.* [9] observed that the photoelastic patterns of running branched cracks initially showed strong mixed mode effects but the mode II effect weakened as the cracks propagated, and eventually approached $K_{II} = 0$.

Following an extensive series of experiments on Homalite-100 using the method of caustics and high-speed photography, Ravi-Chandar and Knauss [11] pointed out that previously published analytical attempts to establish a necessary condition for branching typically compared the states of stress prior to and after the branching event. This treatment did not provide a physical mechanism by which crack branching was achieved. Instead, they proposed the following crack branching mechanism, which is essentially in agreement with the above discussion. When K_I becomes sufficiently high, voids or other material flaws in the crack tip region start to grow themselves into micro-cracks ahead of the main crack front, which effectively becomes an ensemble crack front. The course of further crack propagation and its branching behaviour is then governed by the details of the interaction of these micro-cracks, which continuously communicate through stress waves. Most micro-branches only extend part way through the thickness of the specimen, and vary in size so that the larger ones are most likely to develop into fully-fledged branches, while others are arrested as a result of dynamic interaction with the growing ones. This observation points to statistical effects in branching, which were indeed evident in their experiments.

In a later study, Arakawa and Takahashi [12] attempted to correlate fracture surface roughness and the onset of successful branching in brittle polymers with the crack speed and the dynamic stress intensity factor. Tests were performed on three different materials using a specimen geometry that allowed both acceleration and deceleration of the crack tip. The results conclusively showed that, in fact *neither* parameter individually correlated with the experimental observations. However, a good correlation existed between the surface roughness and a new parameter, $R^* \cdot v$, where R^* is related to the dynamic energy release rate and v is the crack velocity. This parameter has the dimensions of energy flux per unit crack width per unit time and is essentially a measure of the power consumed in the crack tip region. In a further study [13], these authors observed that the new parameter, $R^* \cdot v$, accurately predicted the onset of branching in the same specimen geometries.

In an attempt to perform high resolution velocity measurements without interfering with the dynamics of the crack tip, Fineberg *et al.* [14], Sharon *et al.* [15-18], Hauch and Marder [19], and Ivankovic *et al.* [20-22] used a conductive strip technique to determine the velocity of the crack tip. Fineberg *et al.* [14] reported that when the crack velocity in the PMMA specimens exceeded a critical value v_c=330±20 m/sec (approx. 0.36 times the Rayleigh wave speed, c_R), a dynamic instability was observed. Below v_c, the velocity increased smoothly and the surface was featureless on scales larger than 1 µm. Above v_c, a surface pattern was observed, accompanied by high frequency velocity fluctuations. The surface profile subsequently developed into a coherent, banded structure with a wavelength of the order of 1 mm in the crack propagation direction. In PMMA, these patterns initiated within the 'mist' region where their width was much less than the thickness of the sample. As crack propagation proceeded, however, the width of these surface features increased until

eventually, within the 'hackle' zone, they extended across the entire thickness of the sample. These patterns were not smooth undulations along the fracture surface, but were discrete bands of jagged cliff-like structures [23]. A similar observation was made in earlier investigations by Doll and Weidmann [24], Kusy and Turner [25], and Doyle [26]. Further investigation by Sharon *et al.* [17] confirmed that the surface structure was a result of micro-branch formation. As the crack velocity increased, these structures increased in height and existed up to the point of macroscopic crack branching. It was also found that the apparent dramatic increase of fracture resistance with crack length could be accounted for by considering the effective area of the subsurface damage [18]. The value of v_c, was found to be independent of the sample geometry, sample thickness, applied stress, surrounding atmosphere, and acceleration rate of the crack [23]. Recent tests performed by Livne *et al.* [27] on dynamic fracture of polyacrylamide gels reproduced many of the features of the previous investigations. However, the range of crack tip acceleration rates obtained in these tests was an order of magnitude higher than those observed with the more traditional materials. It was found that the critical velocity increased systematically with the mean acceleration, from 0.34 c_R at lower rates to 0.75 c_R at high rates, suggesting a constant characteristic activation time for the material.

In this paper, an investigation of the branching characteristics of small PMMA single edge notched tensile (SENT) specimens is presented. Of particular interest are the experimental conditions under which successful branching occurred as a function of notch length and specimen thickness. In an attempt to gain further insight into the phenomenon of branching, numerical simulations were performed which accounted for the initiation, growth and interaction of micro-cracks in the vicinity of the main crack tip. To this end, a cohesive zone methodology was employed together with a finite volume formulation, which together provide a simple, robust solution for problems of this kind.

2. Experimental procedure and test results

2.1. Specimen preparation and preliminary tests

The SENT specimens were manufactured from large PMMA sheets used primarily for glazing and commercial purposes. All specimens were produced from the same sheet to eliminate batch variations. Sheet thicknesses of both 3 mm and 8 mm were used. The relatively small specimen geometry shown in Fig. 1 was used as it was sufficiently wide to enable fully branched cracks to develop, whilst being small enough to allow accurate simulations to be carried out by the finite volume (FV) software. The specimens were cut to size and finished on a milling machine and the edges were polished with emery paper. The head of the milling machine was then rotated through 45 degrees and notch depths of 0.1 mm, 0.15 mm, 0.5 mm, 1.0 mm, 1.4 mm and 2.0 mm were machined. An optical profile projector was used to check the depth and quality of the notches. Typical notch tip radii of the order of 30 μm were observed.

The upper and lower 30 mm were inserted into the grips of the tensile testing machine to provide a gauge length of 63 mm. The Young's modulus, Poisson's ratio and density of the material were taken as 3.24 GPa, 0.35 and 1190 kg/m^3 respectively, and so the longitudinal wave speed was 2090 m/sec in this case. Under these conditions, a gauge length of 63 mm was sufficient to prevent interaction between

reflected waves from the top and bottom of the specimen and the crack tip when the latter is travelling at a velocity of the order of 800 m/sec. These very high crack velocities have been observed by Ivankovic and Hillmansen for SENT specimens containing notch depths of 0.1 mm [20] in which branching had occurred. The tests were carried out at an extension rate of 2 mm/min.

Preliminary tests were performed on both sets of specimens to establish if and when branching occurred. Unfortunately, it was found that the 3 mm thick specimens failed to exhibit successful branching for any of the notch depths considered. Some attempted crack bifurcation was observed for the 0.1 mm notches, but it was concluded that the thinner, plane stress specimens were unsuitable for this study. Fortunately, successful branching was readily observed for the thicker 8 mm specimens containing the smaller notch depths, as described below. This observation is somewhat puzzling as the condition for plane strain LEFM requires the specimen thickness to exceed $2.5(K_{IC}/\sigma_y)^2$, where K_{IC} is the fracture toughness and σ_y is the yield strength at the temperature of interest. Fracture toughness values typically range from 0.7 to 1.4 MPam$^{1/2}$ and assuming a yield strength at room temperature of the order of 100 MPa, this suggests that plain strain conditions should certainly be achieved for thicknesses exceeding 0.5 mm. This point remains to be explored. One explanation concerns the effects of bending experienced in SENT specimens at longer crack lengths. It is certainly possible that the bending component might thwart bifurcation in the 3 mm specimens but may have a negligible effect in the 8 mm material.

2.2. Static test results for 8 mm thick specimens

Six to eight valid tests were carried out for each notch depth. The variation of fracture stress with notch depth is shown in Fig. 2 along with the LEFM prediction corresponding to a plane strain fracture toughness of K_{IC} = 0.71 MPam$^{1/2}$, or equivalently, a fracture resistance of G_{IC} = 133 J/m^2. Although this is at the lower end of the normally quoted range of toughness values for PMMA at room temperature [28], it is not particularly surprising as this was an inexpensive, low grade material. In addition, tensile tests were performed in accordance with BS ISO 527-1 1996 to determine the tensile strength of the material. A mean value of 60 MPa was obtained with a standard deviation of 5.5 MPa.

2.3. Branching characteristics of 0.1 mm and 0.15 mm notch depths

Successful macroscopic branching was observed in all six of the 0.1 mm and in four out of six of the 0.15 mm notch depths tested, as shown in Figs. 3 and 4. In all other cases, the fracture surface was essentially flat, as shown in Fig. 5. In these photographs, the specimens were placed on a textured fabric and lit obliquely to enhance the contrast of the images. Although there is clearly a large statistical variation in the branching patterns, some general observations may be made.

In many cases, macroscopic branching typically occurs at an angle of 25 degrees to the horizontal. See, for example Fig. 3(c) and Figs. 4(a)-(c). In some cases, however, larger or smaller angles are observed. For example, one of the arrested branches in Fig. 3(a) is inclined at 45 degrees to the horizontal, whilst the lower fracture surface in Fig. 3(f) is approximately horizontal.

Another striking feature is the feathery nature of the fracture surfaces. Each macroscopic branch is associated with many small cracks along its length representing sequential unsuccessful branching attempts. As noted above, this rapid increase in fracture surface area accounts for the steep rise in apparent dynamic fracture toughness in PMMA at high crack velocities.

In addition, the majority of the individual cracks are rather straight at this level of observation. The successful branches do level off as they approach the right hand face of the specimen, but most of the shorter attempted branches do not exhibit substantial curvature.

The main results are summarized in Tables 1 and 2. Branching distances were measured along the fracture surface itself. Clearly, on average, branching occurs earlier in the specimens containing the shorter notches. Although the crack velocities were not measured in this case, it is of interest to examine the equivalent static stress intensity factor at the point of branching for each specimen. For the SENT specimen, this takes the form of [28]

$$K_I = Y\sigma\sqrt{a}, \tag{1}$$

where σ is the remote axial tensile stress, a is the crack length, and Y is a function of the ratio of the crack length to the specimen width, a/W. The function Y may be expressed in the form of a polynomial, as follows:

$$Y = \sum_{n=0}^{n=4} A_n \left(\frac{a}{W}\right)^n, \tag{2}$$

where $A_0 = 1.99$, $A_1 = -0.410$, $A_2 = 18.70$, $A_3 = -38.48$, and $A_4 = 53.85$.

As shown in Tables 1 and 2, the mean values of K_{Ib} at the point of successful branching are in close agreement for these notch depths. Given that the crack velocities for these specimens are likely to be very similar, this would concur with the previous observations discussed in Section 1 that branching occurs at a critical stress intensity factor under these conditions.

2.4. Visual inspection of fracture surfaces

Typical fracture surfaces for each notch depth are shown in Fig. 6. In general, as the notch depth increases corresponding to a reduction in the failure stress, the size of the mirror region increases and the fracture surface roughness decreases. The mirror region always takes the form of a thumbnail shape whose maximum extension is summarised in Table 3. For the 0.1 mm notches (Fig. 6(a)), crack propagation appears to commence at the lower right hand corner of the image. The initial 0.75 mm of featureless fracture surface quickly gives way to the characteristic banded structure described above. The ordered bands are then succeeded by a rougher hackled region, which subsequently increases in roughness until branching occurs. The behaviour of the 0.15 mm notches is similar, with a larger mirror region of 1.0 mm and a slightly smoother banded structure. The mirror region associated with the 0.5 mm notches is 2 mm and the banded structure exists for approximately 8 mm, after which the hackle region begins. Here, no branching occurs. The fracture surfaces corresponding to the larger notches display the banded structure for the entire mist region, although the

roughness associated with the 2 mm notches (Fig. 6(f)) is visibly less than that observed with the other specimens.

2.5. Scanning electron microscopy of fracture surface

The specimen shown in Fig. 7 was chosen to demonstrate the evolution of the fracture surface topology in the direction of crack propagation for cases in which successful branching occurred. Fig. 8 contains the sequence of scanning electron micrographs along the centre of the upper fracture surface from the left (a) to the right hand edge (h). As noted above, the mirror region here is semi-circular and extends for approximately 0.75 mm. At higher magnifications, the well-reported parabolic marks could be seen in this region. The mist region then consists of about seven concentric bands for a further 1.5 mm, beyond which the surface becomes disordered and the roughness increases steadily until successful branching occurs after about 6.6 mm at the right hand side of Fig. 8(b). During the next 13 mm of the branching event (Figs. 8(c)–(f)), the fracture surface changes its appearance quite dramatically as substantial crack curvature occurs. Thereafter, for the final 6 mm (Figs. 8(g)-(h)), the appearance of the surface is very similar to the way it was before the branching event, becoming smoother as the right hand edge is approached.

2.6. Subsurface damage

A typical specimen containing a 0.1 mm notch was then sectioned along planes perpendicular to the initial fracture surface and examined under the SEM for evidence of subsurface damage. The cross-sections chosen were located 1.5 mm, 7 mm, and 13 mm after the branching event and the resulting micrographs are shown in Fig. 9. In the first cross-section, Fig. 9(a), very little damage beneath the primary fracture surface was evident. The only visible crack occurred at a depth of 100 μm below the surface. In the second cross-section, Fig. 9(b), subsurface damage had increased in magnitude and frequency and cracks were observed at depths of over 400 μm. Finally, after 13 mm of branching, the extent of subsurface damage has increased further, with layers of damage occurring up to 2 mm below the fracture surface. Fig. 9(c) shows one such layer 0.6 mm below the surface.

3. Numerical simulations

3.1. Background

Branching typically takes place at relatively high crack tip velocities. Early analytical investigations into the cause of branching, such as that presented by Yoffe [29], focussed on the evolution of the asymptotic stress field ahead of a dynamically propagating crack. However, whilst there is no doubt that the nature of the stress field ahead of a rapidly moving crack must have a considerable role to play, such analyses do not adequately predict whether or not branching will occur, and if so, under what conditions it will take place. Alternative, energy-based approaches, such as those considered by Eshelby [30], and recently by Adda-Bedia [31], examine the conditions under which sufficient energy will be available to drive two slower crack tips instead of a single fast one. Whilst this must be seen as a necessary condition for branching, a key assumption of such analyses is the reduction in the velocity of the two new crack

tips immediately after the branching event, which, as mentioned above is not seen in practice.

The failure of these analytical models to adequately explain experimental observations lies primarily in the assumption that the dimensions of the fracture process region are considered to be negligible in comparison to the crack length and that the crack tip simply acts as an energy sink during crack propagation. As noted in Section 1, however, the dynamic evolution of the process region ahead of the running crack is of fundamental physical importance and plays a key role in determining the macroscopic behaviour of the crack.

3.2. Model description

A finite volume formulation was used to simulate the dynamic fracture of the 25×63 mm PMMA specimens [21, 22, 32, 33]. Traction free boundary conditions were applied to the left and right hand edges of the model, the bottom edge was held fixed, whilst the displacement (static analyses) or the velocity (transient analyses) were specified along the top edge. A uniform fine grid region was defined, which spanned the width of the model and whose height extended an equal distance above and below the initial fracture plane. The appropriate height of the fine grid region depended on the notch depth, and had to be large enough to contain the evolving fracture process zone. For the smallest notches, the height of this region was chosen to be 20mm. Within the fine grid region, a square cell size of 20×20 µm was used. Outside this region, the height of the cells increased gradually to 0.8 mm at the top and bottom of the model. The number of continuum cells in these models exceeded 1.3 million. Plane strain conditions were assumed. The use of 20 µm cells in the fine grid region meant that the 0.15 mm notch could not be modelled exactly. Instead, a 0.16 mm notch was simulated.

The analysis procedure may be summarized as follows. At the end of a given time step, the tractions across the faces of each continuum cell were evaluated and if the failure criterion was satisfied anywhere in the model, cohesive cells were inserted between the continuum cells adjacent to this face. The time step was then repeated so that a converged solution was obtained for the model containing the recently added cohesive cells before proceeding to the next time step. In this investigation, a purely tensile failure criterion was assumed. Hence the cohesive cells were inserted if the normal traction was greater than or equal to the cohesive strength.

The cohesive characteristic chosen for this investigation is shown in Fig 10. The cohesive strength and the fracture energy were taken as 80 MPa and 133 J/m^2, respectively. As noted above, failure stresses of up to 65 MPa were observed in the unnotched tensile tests. Given the imperfect surface finish of these specimens, it seems reasonable to assume a cohesive strength of 80 MPa. The fracture energy was determined by the application of LEFM to the SENT data, as shown in Fig. 2. Together, these values provided good agreement with the experimental observations, as shown below.

It was shown in a previous investigation that the shape of the cohesive law has a profound influence on analyses of this kind [22]. The cohesive law chosen here is phenomenological in nature and is based on an inverse procedure whereby the shape was adjusted until the dynamic behaviour of the model was in good agreement with experimental observation [22]. As in the previous investigation, the cohesive behaviour may be summarized as follows. When the normal opening displacement δ increases monotonically, the normal cohesive traction σ decreases according to the

cohesive law in Fig. 10. If, after some opening displacement δ^*, unloading takes place, then the tractions obey a linear unloading relation through the origin. If subsequent reloading takes place, the unloading path is reversed until the displacement δ^* is reached, and subsequently the monotonic cohesive relations are followed again. When the critical normal separation is reached, fracture is assumed to have taken place and the cell faces are thereafter treated as traction-free surfaces. Although subsequent contact of the fracture surfaces is not taken into account, this is not considered to be of primary importance in this case.

The shear traction across the cohesive surfaces is computed as follows. Before the cohesive cells are inserted between the faces of the adjacent continuum cells, the prevailing shear traction on this plane is noted. Although the initial shear traction associated with each cohesive surface will, in general, be different for different cells, let this value be denoted as τ_o. After the cohesive cells have been inserted, the shear traction corresponding to a given normal traction σ is simply taken to be $\tau = (\sigma/\sigma_{coh})\,\tau_o$, where σ_{coh} is the cohesive strength of the material. Hence, the shear characteristic has the same shape as the normal characteristic. This is essentially the same cohesive behaviour as assumed by Camacho and Ortiz [34].

3.3. Static results

In the static phase of the analysis, the model was loaded by applying displacement increments to the top face. When the traction across the cell face directly ahead of the crack tip reached the cohesive strength, a cohesive cell was inserted between the adjacent continuum cells, as described above. This procedure continued until the point where unstable crack growth was imminent, when the magnitude of the applied incremental displacements was considerably reduced to allow the final stages of cohesive zone formation to be accurately modelled. Eventually, the analysis failed to converge and the static results were recorded. The predicted values of failure strength are compared with the experimental observations in Table 4. Clearly, very good agreement exists between the two sets of data.

3.4. Dynamic results

The subsequent rapid crack propagation phase was then simulated for the 0.1, 0.16, and 0.5 mm notch depths, and the results are presented below. In each case the top face of the model was subjected to the experimental loading rate of 3.3×10^{-5} m/s (or 2 mm/min). Results of particular interest from the transient analysis include the occurrence of successful branching as a function of notch depth, the mechanism of branch formation, and the increase of the apparent dynamic fracture resistance of the material as a result of micro-crack formation in each case.

The damage evolution in the fine grid region of each model is shown in Fig. 11. The corresponding crack speed histories are shown in Fig. 12. For clarity of presentation, the simulated crack speed histories in Figs. 12(a)-(c) were smoothed using a 0.075 μs time-window. In Fig. 12(d), the same data is presented, but here the high frequency oscillations have been smoothed out using a 1.0 μs time-window, and the mean velocities may be compared more easily. For each notch depth, the crack growth is characterised by a period of initial acceleration up to a mean terminal velocity below the Rayleigh wave speed. During the initial period of propagation, the crack is confined to its original plane and the fracture surface in this region is flat with

no visual subsurface damage. Thereafter, the extent of the subsurface damage increases and the crack speed exhibits characteristic high frequency oscillations. The rate of the initial acceleration clearly decreases as the notch depth increases, as observed experimentally by Ivankovic and Hillmansen [20]. The 0.1 mm and 0.16 mm notches are predicted to reach a similar mean terminal velocity of about 820 m/sec, whilst the 0.5 mm notch is predicted to propagate at a slightly lower value of 760 m/sec. It should be noted that while the former value agrees well with previous experimental measurements [20], the terminal velocity of the longer notch is overestimated by about 50%. This might be attributed to the fact that the current analysis is two dimensional and fails to capture the fully three dimensional evolution of the fracture process.

Perhaps the most striking observation about Fig. 11 is that successful branching is only predicted for the 0.1 and 0.16 mm notches. No branching is predicted for the 0.5 mm notch, in agreement with the experimental investigation. In addition, the comparison presented in Table 5 shows that the predicted branching location lies within the experimental range for both notch depths. Indeed the general appearance of the predicted branching patterns is quite similar in form to the experimental photographs. Compare, for example, Fig. 11(b) and Fig. 4(b) for the 0.15 mm notch, and Fig. 11(c) and Fig. 3(c) for the 0.1 mm notch. One obvious difference is the overestimation of the branching angles, as discussed below.

It is also of interest to observe the evolution of the fracture surface area as a function of notch depth. The formation of micro-cracks and successful branches both contribute to the increase in actual fracture surface area and hence the effective dynamic fracture resistance of the material. As shown in Fig. 13, the final fracture surface area is approximately twice the cross-sectional area of the specimen in the case of the 0.5 mm notches, corresponding to the modest formation of micro-branches and subsurface damage shown in Fig. 11(a). This rises to a factor of seven for the 0.16 mm notches, and a remarkable factor of 12 for the 0.1 mm notches.

Finally, the mechanism of macroscopic branch formation may be examined in more detail. Fig. 14 shows the typical sequence of events leading to successful branching. Here, the field of view is 1 mm by 1 mm ahead of the rapidly propagating crack tip. Of course it must be emphasised that the specific results shown in this figure are mesh dependent. Micro-crack formation is only possible along horizontal or vertical planes and a relatively coarse cell size of 20 μm has been employed. Nonetheless, similar overall behaviour would be expected with a finer, unstructured mesh.

Firstly, the size of the fracture process region grows laterally while the main crack extends along the original horizontal plane (Fig. 14(a)-(b)). Then, the plane of propagation changes slightly and 10 micro-cracks are formed on planes normal to the main propagation direction. In addition, another micro-crack forms on a horizontal plane above and 160 microns ahead of the main crack tip. This will prove to be the seed crack for the branch formation (Fig. 14(c)). The process region continues to evolve, and a total of 23 lateral micro-cracks on vertical planes have formed, while the horizontal seed crack grows at an inclined angle, here approximately 45 degrees (Fig. 14(d)). The upper and lower branches are now fully established and continue to grow. The main horizontal crack effectively arrests and a new coplanar horizontal crack opens up approximately 160 microns ahead of the original tip and propagates forwards and backwards, leading to coalescence at the branching point (Fig. 14(e)-(f)).

9

3.5. Discussion

Comparing Figs. 3 and 4 to Fig. 11, it can be seen that the overall branching angles are overestimated in the finite volume simulations. It is likely that a more rigorous mixed-mode analysis would lead to increased crack curvature, as discussed in Section 1. Also, it should be emphasised that the shape of the cohesive law has a great effect on the simulation results. This is to be expected, of course, as the traction-separation law reflects the microscopic processes that are taking place during failure of the material and is typically dependent on the structure of the material as well as the rate of separation, the degree of constraint and the temperature at which the cohesive law is determined.

The behaviour of the model is essentially in agreement with a recent discussion by Broberg [35] on the significance of morphology changes of the process region ahead of a rapidly propagating mode I crack. In this paper, it is noted that in the vicinity of the dynamic crack tip, the normal stress on planes perpendicular to the direction of crack growth is larger than the opening stress along the crack plane. This is predicted to lead to a significant lateral expansion of the process region, with the formation of micro-separations in directions other than that of the main crack.

4. Conclusions

The simulations proved very useful in providing insight into the mechanism of branch formation, which was fully in accordance with previous experimental investigations. It was confirmed that the evolving morphology of the expanding fracture process region plays a fundamental role in determining the macroscopic behaviour of the running crack. Successful branching appears to take place when micro-cracks form a sufficient distance from the main crack tip to allow their subsequent propagation to take place as opposed to being arrested by the arrival of an unloading wave from the main crack.

Table 1
Experimental observations for the specimens containing 0.1 mm notches.

	Failure Stress (σ) (MPa)	Attempted Branching (mm)	Successful Branching (a_b) (mm)	$K_{Ib} = Y\sigma\sqrt{a_b}$ (MPa m$^{1/2}$)
	37.9	3.0	6.8	8.7
	42.0	2.7	4.6	6.8
	34.4	3.6	8.5	10.2
	32.0	3.3	5.8	6.3
	36.1	2.5	6.9	8.4
	32.8	3.2	7.0	7.8
Mean	35.9	3.1	6.6	8.0
Std. Dev.	3.4	0.4	1.2	1.3

Table 2
Experimental observations for the specimens containing 0.15 mm notches.

	Failure Stress (σ) (MPa)	Attempted Branching (mm)	Successful Branching (a_b) (mm)	$K_{Ib} = Y\sigma\sqrt{a_b}$ (MPa m$^{1/2}$)
	32.2	4.9	9.0	10.3
	33.4	4.3	6.5	7.3
	31.1	3.8	6.3	6.6
	29.4	3.8	6.9	6.8
Mean	31.6	4.2	7.2	7.8
Std. Dev.	1.5	0.5	1.1	1.5

Table 3
Average length of the mirror region as a function of notch depth.

Notch Depth (mm)	0.1	0.15	0.5	1.0	1.4	2.0
Mirror region (mm)	0.75	1.0	2.0	2.5	4.0	4.25

Table 4
Comparison of numerical predictions and experimental observations for SENT tests. Mean experimental values are quoted with the standard deviation shown in brackets.

Notch Depth (mm)	Experimental Stress (MPa)	Predicted Stress (MPa)
0.1	35.8 (3.7)	35.0
0.15	30.2 (3.5)	28.8 *
0.5	16.0 (2.0)	17.1

* Simulation was for 0.16 mm notch

Table 5
Crack lengths at which successful branching occurred.

Notch Depth (mm)	Experimental Range (mm)	Predicted Value (mm)
0.1	4.6 to 8.5	5.6
0.15	6.3 to 9.0	8.6
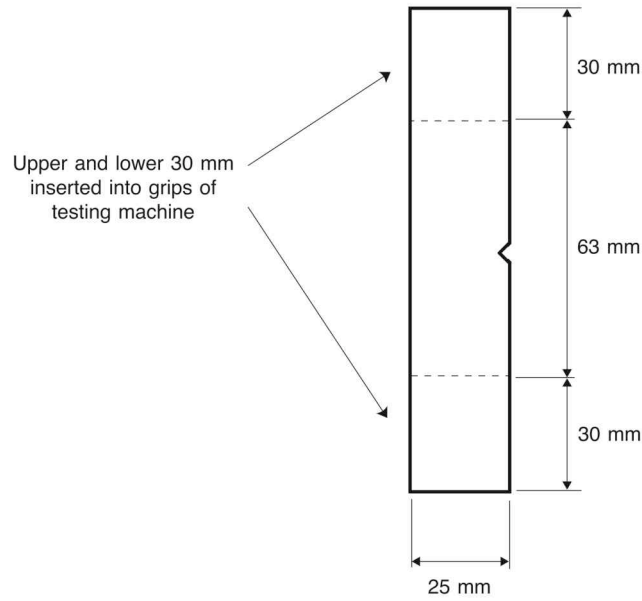
Fig. 1. Overall dimensions of SENT specimens. The upper and lower 30 mm were inserted into the grips of the tensile testing machine, resulting in a gauge length of 63 mm.
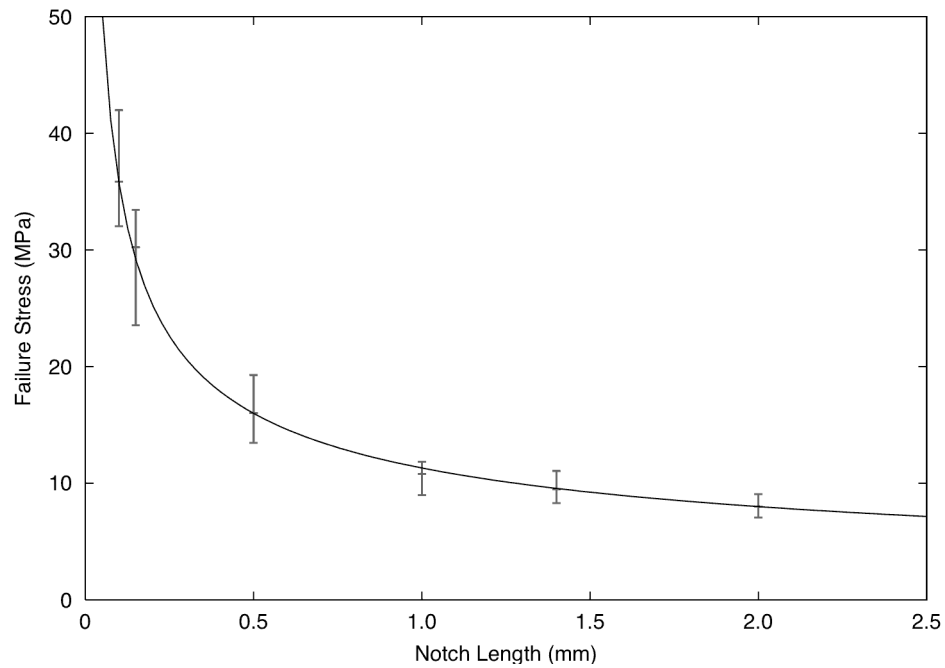

Fig. 2. Static results of SENT tests for 8 mm thick specimens. The vertical error bars show ranges of experimental values for each notch size. Curve shows LEFM prediction for $K_{IC} = 0.71$ MPam$^{1/2}$, or equivalently, $G_{IC} = 133$ J/m^2.
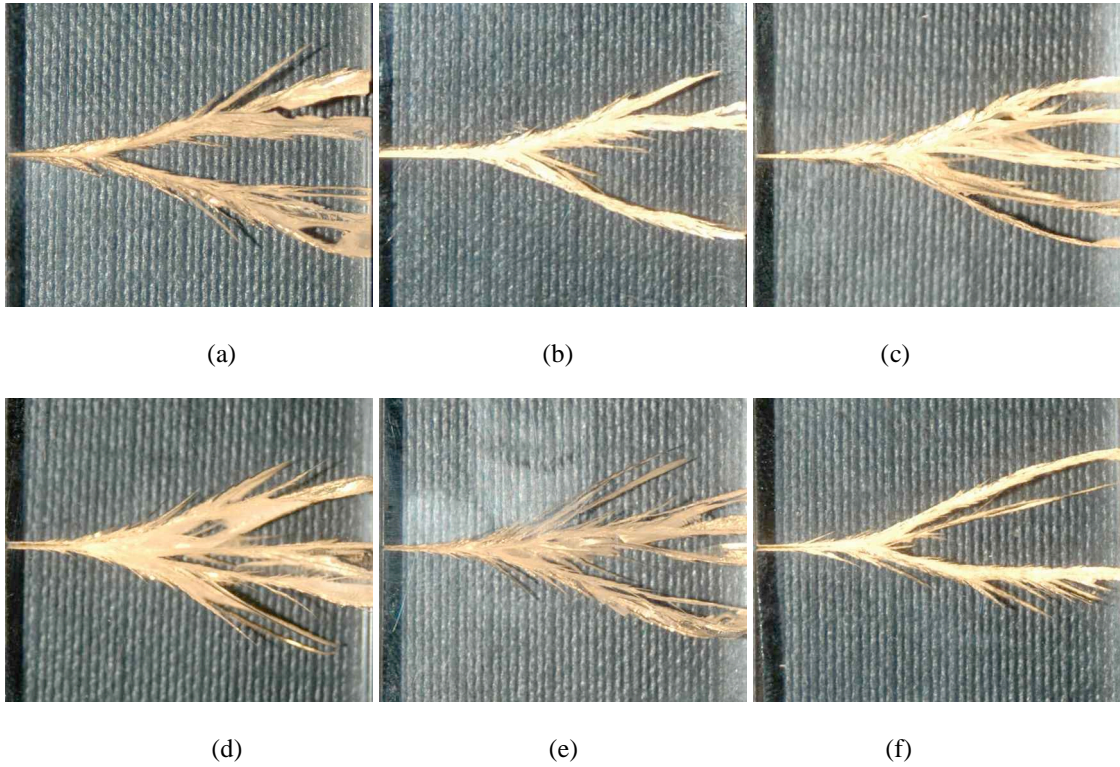
Fig. 3. Branching patterns in specimens containing the 0.1 mm notches. Successful branching occurred in all of the 8 mm thick specimens tested. The size of the images is 25 by 20 mm in each case.
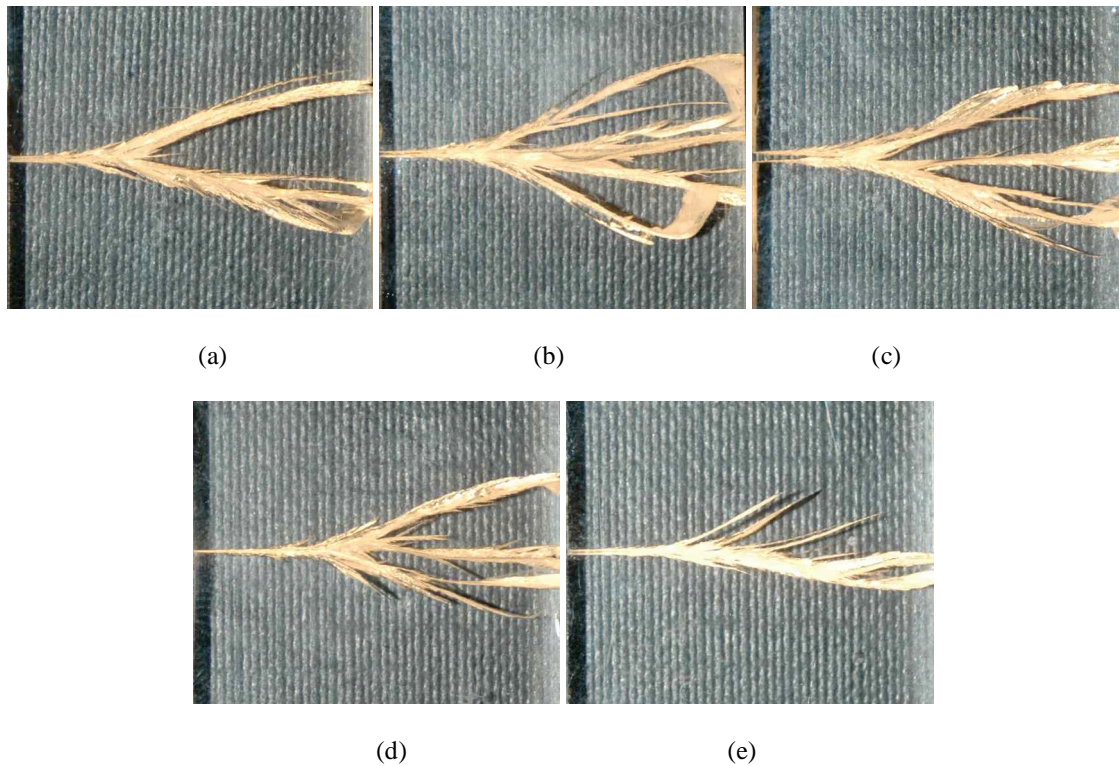
Fig. 4. Branching patterns in specimens containing the 0.15 mm notches. Successful branching occurred in four out of six specimens tested (a) to (d). An unsuccessful branching attempt is shown in (e). The size of the images is 25 by 20 mm in each case.

(a)   (b)   (c)

(d)
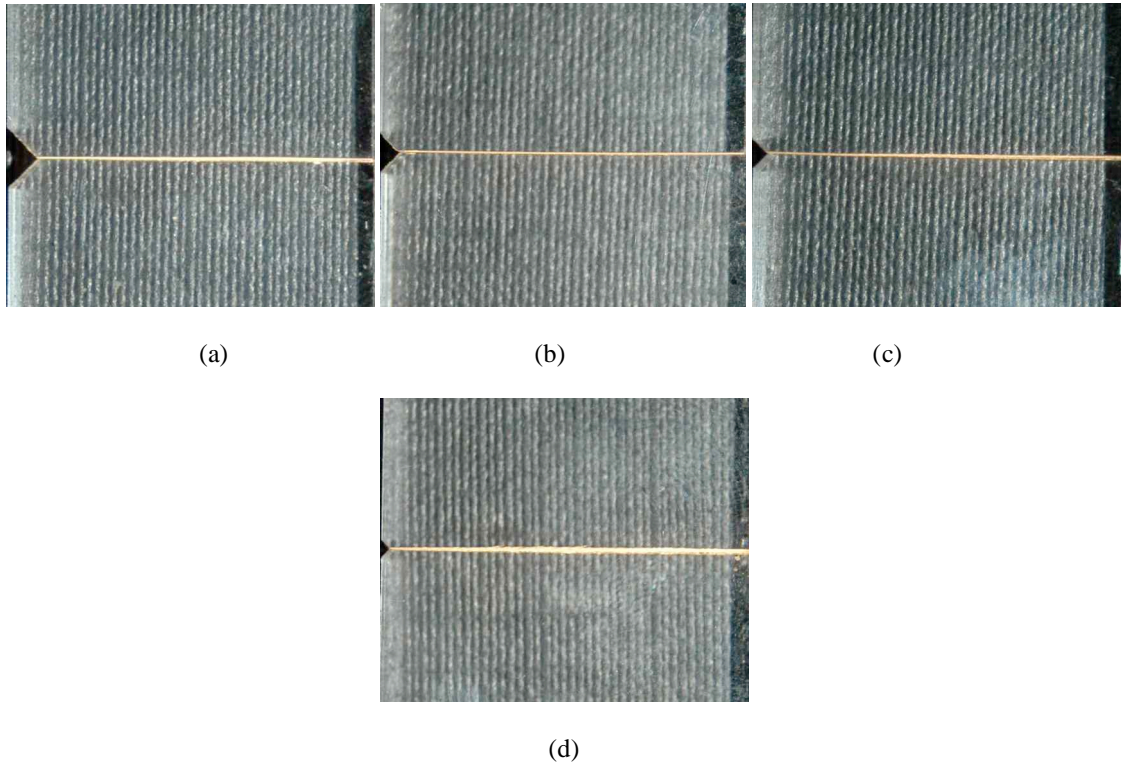
Fig. 5. Macroscopically planar fracture surfaces for the specimens containing the (a) 2.0 mm, (b) 1.4 mm, (c) 1.0 mm, and (d) 0.5 mm notches.

(a)   (b)

(c)   (d)

(e)   (f)
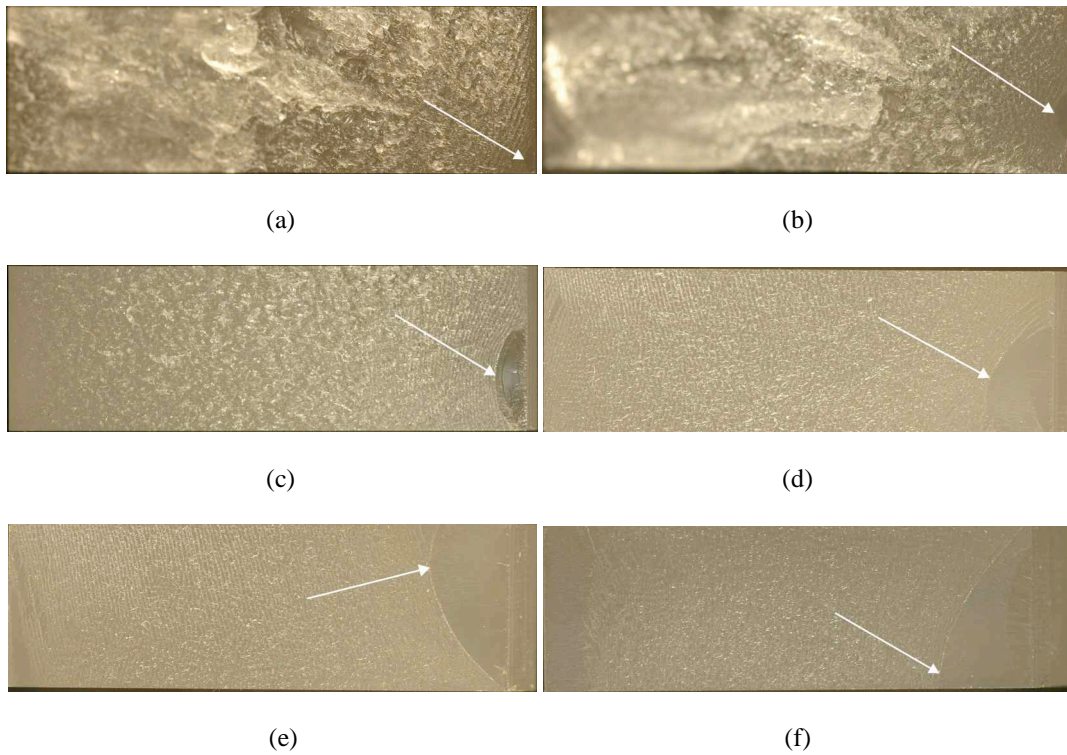
Fig.6. Visual appearance of fracture surfaces for the specimens containing the (a) 0.1 mm, (b) 0.15 mm, (c) 0.5 mm, (d) 1.0 mm, (e) 1.4 mm, and (f) 2.0 mm notches. Note the increase in size of the mirror region with increasing notch depth (arrows show the mirror-mist transition).

Fig.7. Scanning electron micrographs in Fig. 8 traverse the upper fracture surface of this specimen containing a 0.1 mm notch.

(a)

(b)

(c)

(d)

(e)

(f)

(g)

(h)
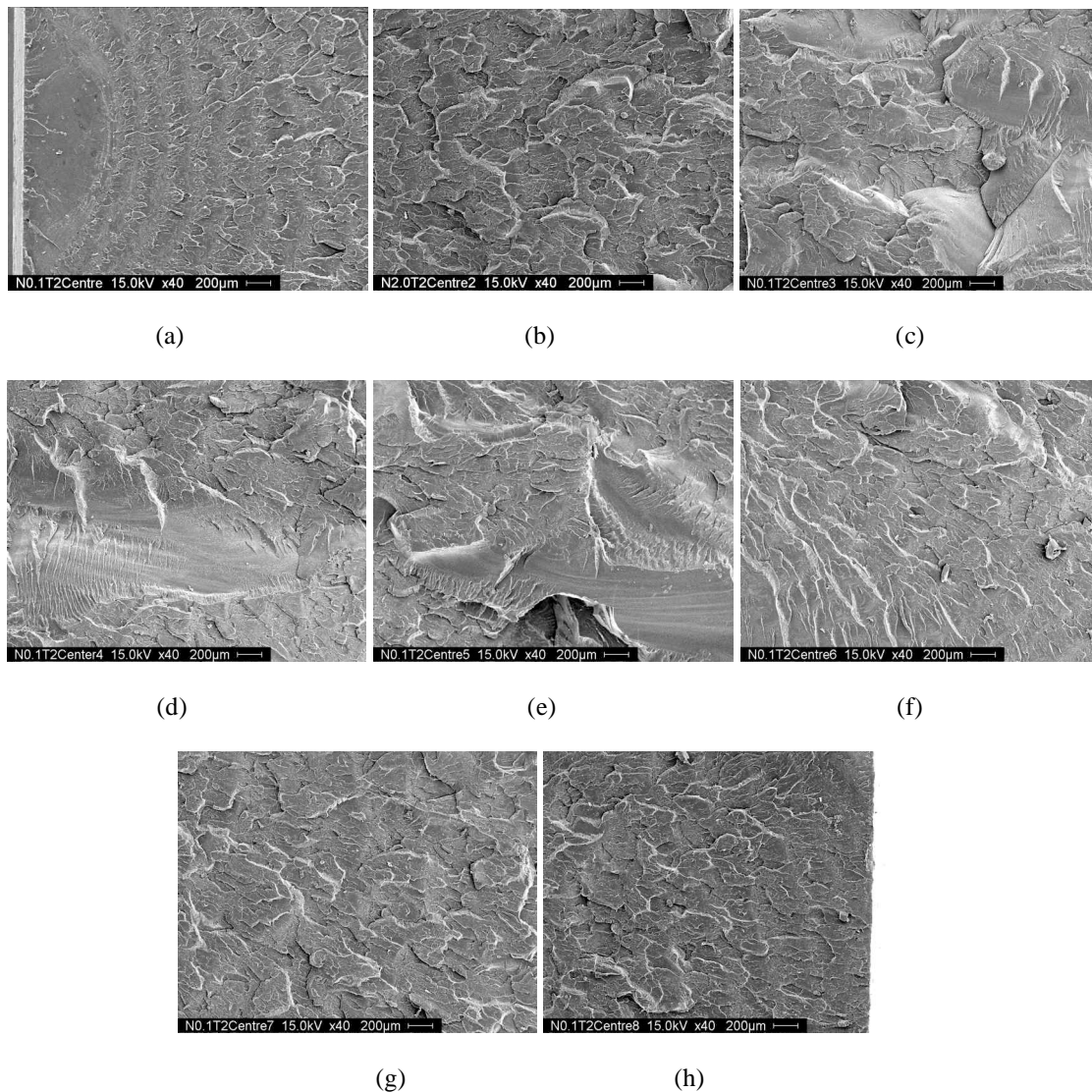
Fig.8. Scanning electron micrographs of upper fracture surface of specimen containing 0.1 mm notch (shown in Fig. 7). The size of each image is 3.25 by 2.55 mm. (a) Crack initiation: mirror-mist transition. (b) Branching occurs towards the end of this image. (c) – (e) During branching event. Significant crack curvature experienced. (f) Approaching the end of crack curvature. (g) – (h) Roughness similar to that immediately prior to branching during the last 5 mm of crack growth, becoming much smoother during the final 0.5 mm.

(a)

(b)

(c)
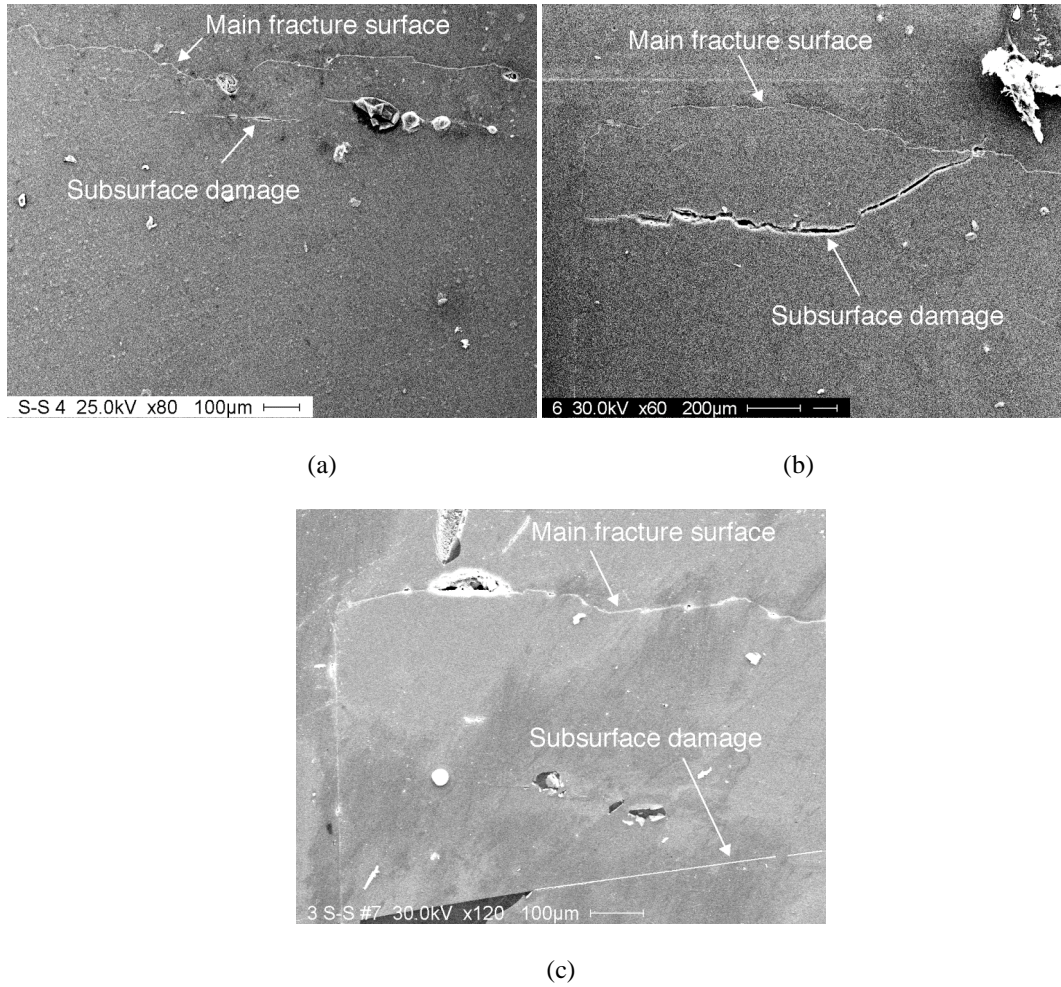
Fig.9. Scanning electron micrographs of subsurface damage associated with 0.1 mm notch. (a) 1.5 mm after successful branching, damage occurs 0.1 mm below main fracture surface. (b) 7 mm after branching, depth of damage increases to 0.4 mm. (c) 12.5 mm after branching, damage is observed 0.6 mm below the surface (this very fine subsurface crack has been enhanced for clarity).
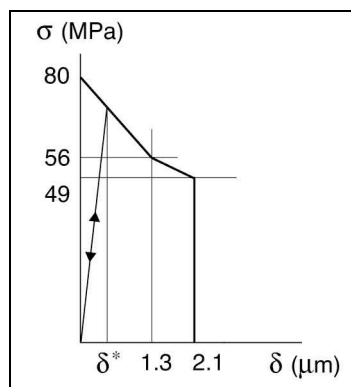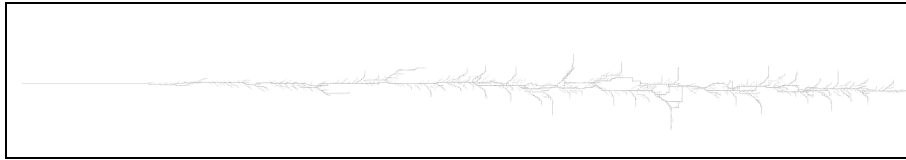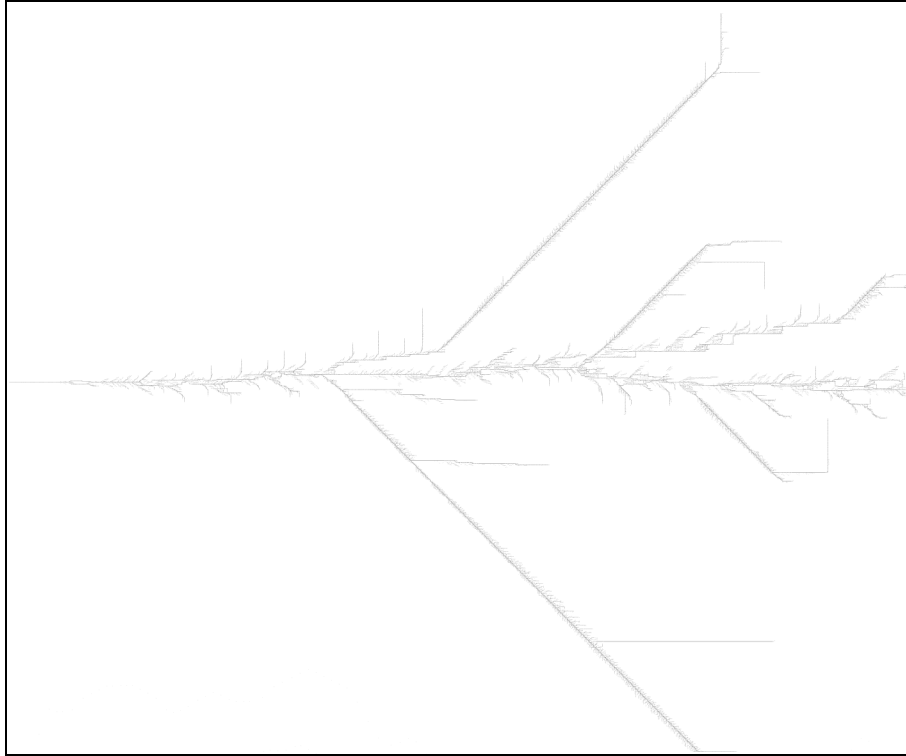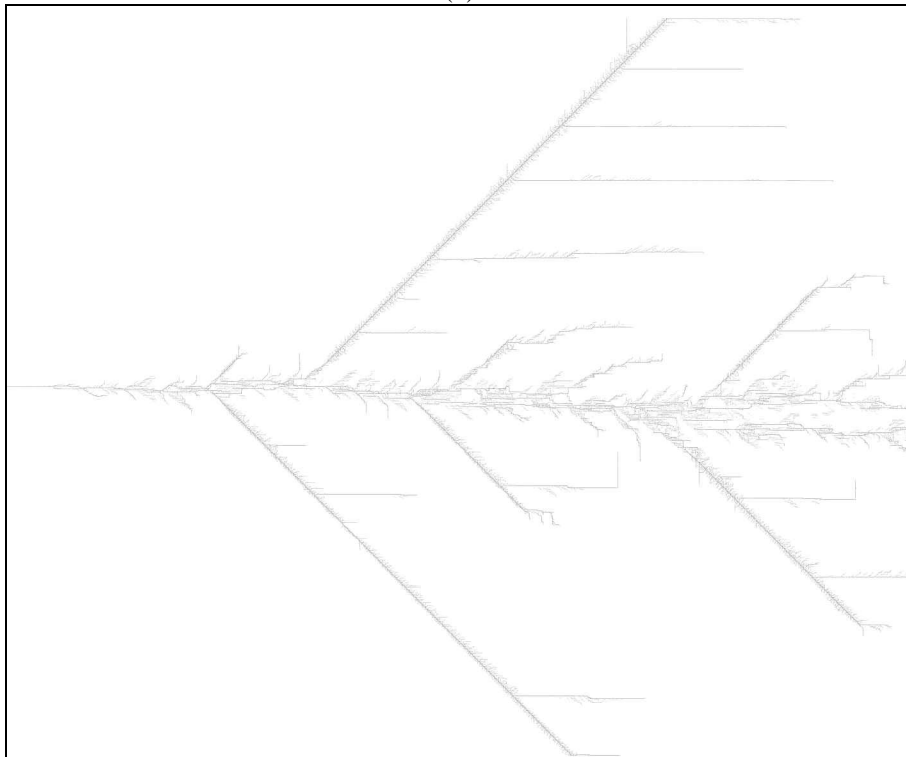

Fig. 10. Assumed cohesive characteristic. The area under the traction-separation curve, G=133 J/m^2.

(a)

(b)

(c)

Fig. 11. Crack path and damage evolution for (a) 0.5 mm, (b) 0.16 mm, and (c) 0.1 mm notches. The sizes of the images in (b) and (c) are 25 by 20 mm, while that of (a) is 25 by 4 mm. Unfortunately, the

17

restriction in the use of colour, coupled with the relatively large amount of information contained in these images makes detailed visual analysis difficult. However, colour images will be included in the online version of this paper where the colour of a given cohesive cell represents its degree of separation.
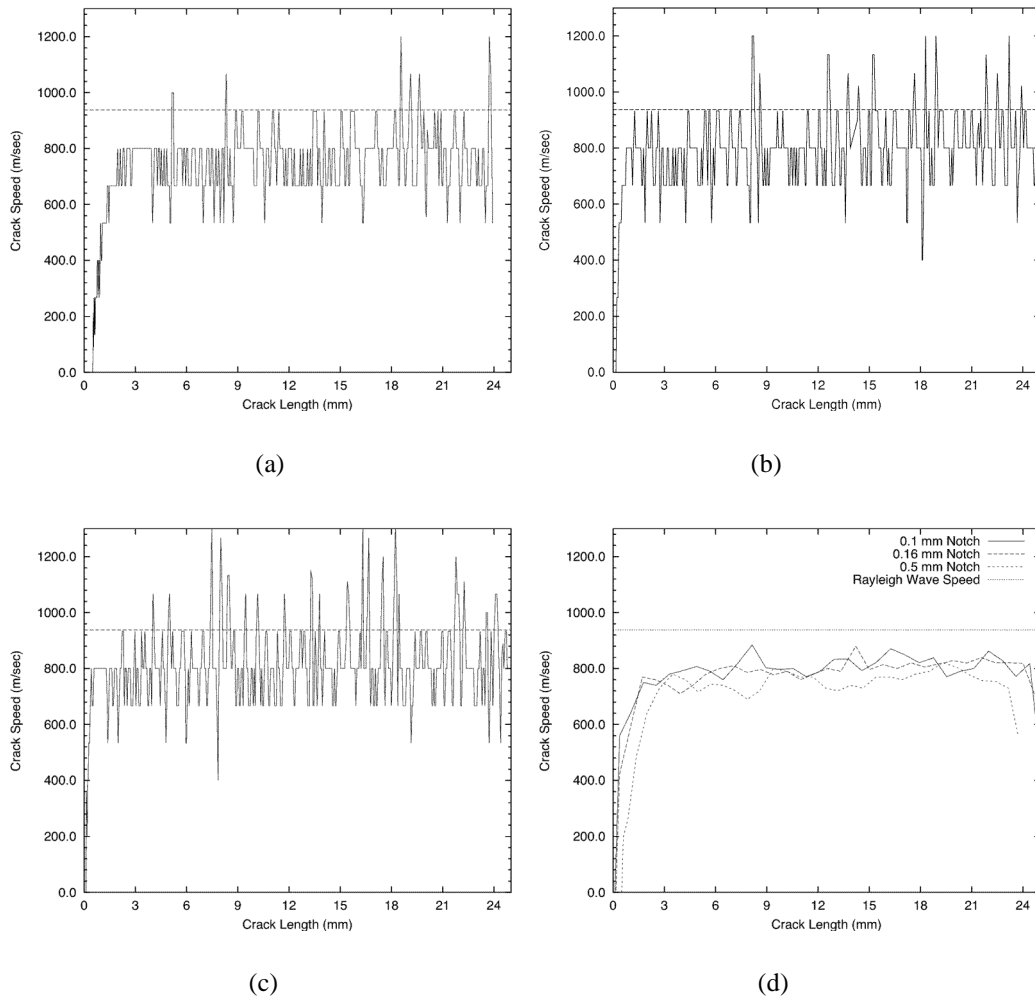

(a)

(b)

(c)

(d)

Fig. 12. Corresponding crack velocity histories for the (a) 0.5 mm, (b) 0.16 mm, and (c) 0.1 mm notches. The Rayleigh wave speed of 930 m/s in PMMA is also shown. Note that artificially high velocities are computed when micro-cracks open up ahead of the main crack tip. (d) Shows the same data but here additional smoothing has been performed to enable the mean velocities to be compared. After branching takes place, there is no longer a single crack tip in the case of the shorter notches. In these cases the crack extension is defined as the furthest distance travelled by either crack. This would then be comparable to the output from the conductive coating experimental technique for velocity measurement, commonly used in practice.
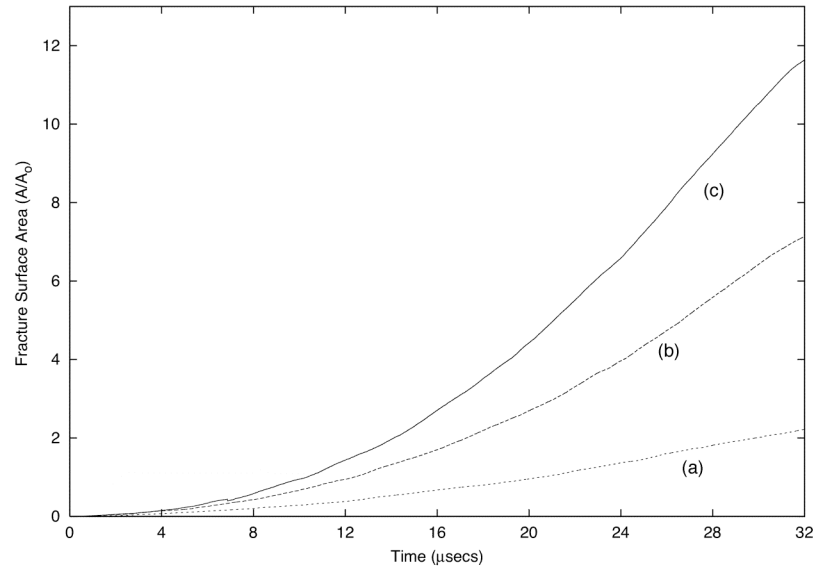
Fig. 13. The evolution of fracture surface area in the case of (a) 0.5 mm, (b) 0.16 mm, and (c) 0.1 mm notch depths. The surface area is expressed in terms of the cross-sectional area of the specimen, A_o.
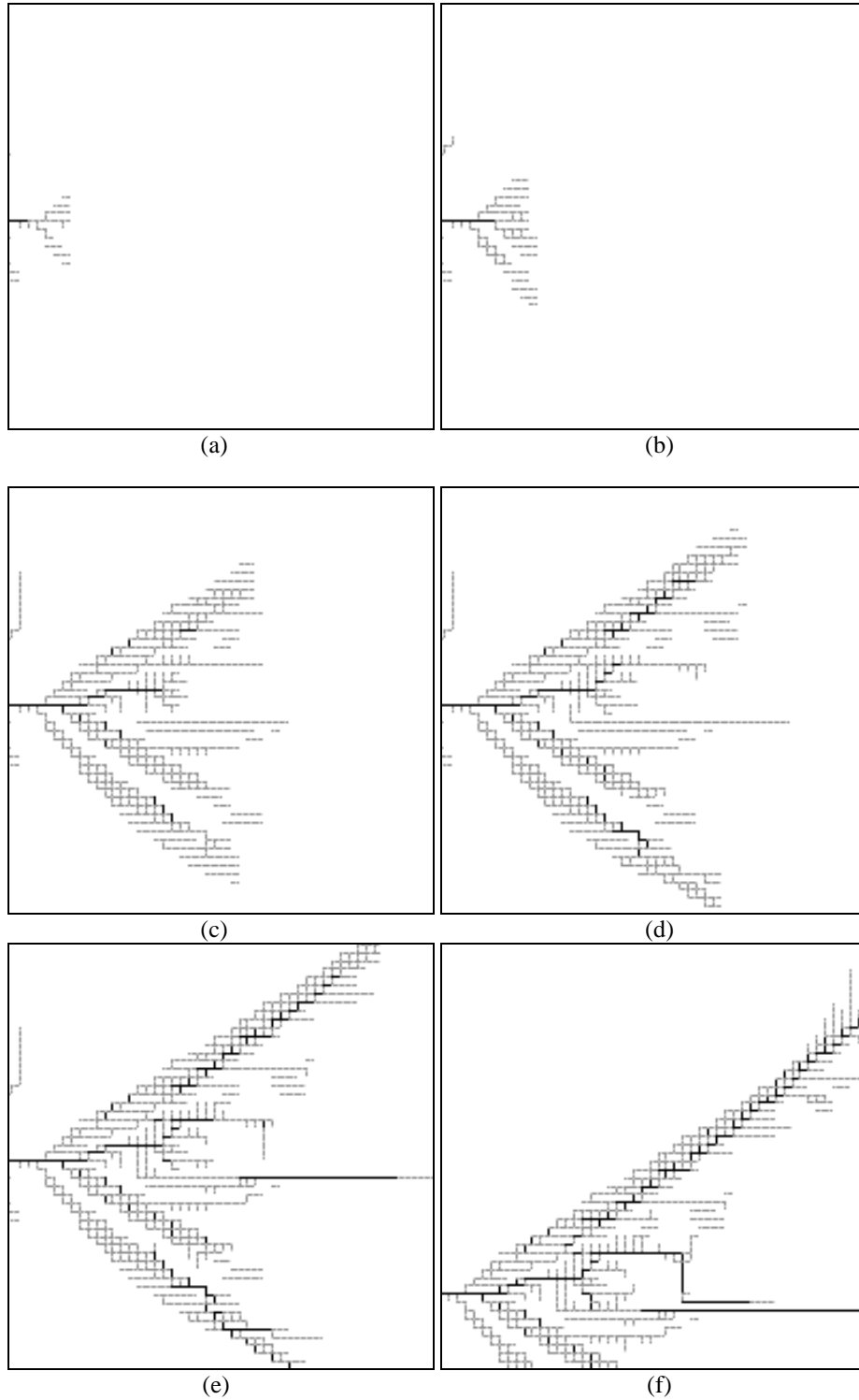
Fig. 14. The development of a typical macroscopic branch. Due to colour restrictions, it is neither possible to show the degree of separation of the cohesive cells nor their status (whether they are being pulled apart or undergoing elastic unloading). These will be shown in the online version of the paper. Instead, cohesive cells that are not fully separated are shown in grey, while fully separated cells are shown in black. Note that only the micro-cracks that form far enough away from the main crack tip subsequently grow into a macroscopic branch, while those close to the main crack tip unload and do not propagate further. As seen in (f), these cracks then effectively grow backwards and coalesce with the main crack tip. Size of windows: 1 mm by 1 mm.

20

References

[1] Schardin H. Velocity effects in fracture. In: Averbach BL, Felbeck DK, Hahn GT, Thomas DA (editors). Fracture. John Wiley & Sons, New York, 1959, p. 297-329.

[2] Clark ABJ, Irwin GR. Crack propagation behaviours. Exp Mech 1966;6:321-390.

[3] Congleton J, Petch NJ. Crack branching. Phil Mag 1967;16:749-760.

[4] Congleton J. Practical applications of crack-branching measurements. In: Sih GC (editor) Dynamic Crack propagation. Noordhoff International Publishing, Leyden, 1973, p. 427-438.

[5] Dally JW. Dynamic photoelastic studies of fracture. Exp Mech 1979;19:349-361.

[6] Streit R, Finnie I. An experimental investigation of crack-path directional stability. Exp Mech 1980;20:17-23.

[7] Cotterell B, Rice JR. Slightly curved or kinked cracks. Int J Fract 1980;16:155-169.

[8] Ramulu M, Kobayashi AS. Dynamic crack curving - a photoelastic evaluation. Exp Mech 1983;23:1-9.

[9] Ramulu M, Kobayashi AS, Kang BSJ, Barker DB. Further studies on dynamic crack branching. Exp Mech 1983;23:431-437.

[10] Kalthoff JF. On the propagation direction of bifurcated cracks. In: Sih GC (editor) Dynamic Crack Propagation. Noordhoff International Publishing, Leyden, 1973, p. 449-458.

[11] Ravi-Chandar K, Knauss WG. An experimental investigation into dynamic fracture: III On steady-state crack propagation and crack branching. Int J Fract 1984;26:141-154.

[12] Arakawa K, Takahashi K. Relationships between fracture parameters and fracture surface roughness of brittle polymers. Int J Fract 1991;48:103-114.

[13] Arakawa K, Takahashi K. Branching of a fast crack in polymers. Int J Fract 1991;48:245-254.

[14] Fineberg J, Gross SP, Marder M, Swinney HL. Instability in the propagation of fast cracks. Phys Rev B 1992;45:5146-5154.

[15] Sharon E, Fineberg J. Microbranching instability and the dynamic fracture of brittle materials. Phys Rev B 1996;54:7128-7139.

[16] Sharon E, Fineberg J. Universal features of the micro-branching instability in dynamic fracture. Phil Mag B 1998;78:243-251.

[17] Sharon E, Gross SP, Fineberg J. Local crack branching as a mechanism for instability in dynamic fracture. Phys Rev Lett 1995;74:5096-5099.

[18] Sharon E, Gross SP, Fineberg J. Energy dissipation in dynamic fracture. Phys Rev Lett 1996;76:2117-2120.

[19] Hauch JA, Marder MP. Energy balance in dynamic fracture, investigated by a potential drop technique. Int J Fract 1998;90:133-151.

[20] Ivankovic A, Hillmansen S. Evolution of dynamic fractures in poly(methyl methacrylate). Plast Rubber Compos 2001;30:88-93.

[21] Ivankovic A, Murphy N, Hillmansen S. Evolution of dynamic fractures in PMMA: experimental and numerical investigations. In: Aliabadi MH, Ivankovic A (editors). Crack Dynamics: Advances in Fracture Mechanics, vol. 9. WIT Press, Southampton, UK, 2005, p. 123-173.

[22] Murphy N, Ivankovic A. The prediction of dynamic fracture evolution in PMMA using a cohesive zone model. Engng Fract Mech 2005;72:861-875.

[23] Fineberg J, Marder M. Instability in dynamic fracture. Physics Reports 1999;313:1-108.

[24] Doll W, Weidmann GW. Transition from slow to fast crack propagation in PMMA. J Mat Sci 1976;11:2348-2350.

[25] Kusy RP, Turner DT. Influence of molecular-weight of poly(methyl methacrylate) on fracture morphology in notched tension. Polymer 1977;18:391-402.

[26] Doyle MJ. A mechanism of crack branching in polymethyl methacrylate and the origin of the bands on the surfaces of fracture. J Mat Sci 1983;18:687-702.

[27] Livne A, Cohen G, Fineberg J. Universality and hysteretic dynamics in rapid fracture. Phys Rev Lett 2005;94:(224301).

[28] Williams JG, Fracture mechanics of polymers. Ellis Horwood; 1984.

[29] Yoffe EH, The moving Griffith crack, 1951, 739-750.

[30] Eshelby JD, Energy relations and the energy-momentum tensor in continuum mechanics, 1970, 77-115.

[31] Adda-Bedia M. Brittle fracture dynamics with arbitrary paths III. The branching instability under general loading. J Mech Phys Solids 2005;53:227-248.

[32] Demirdzic I, Muzaferija S. Finite volume method for stress analysis in complex domains. Int J Num Meth Eng 1994;37:3751-3766.

[33] Ivankovic A. Finite volume modelling of dynamic fracture problems. Comput Model Simulat Engng 1999;4:227-235.

[34] Camacho GT, Ortiz M. Computational modeling of impact damage in brittle materials. Int J Solids Struct 1996;33:2899-2938.

[35] Broberg KB. Significance of morphology changes at a propagating crack edge. Int J Fract 2004;130:723-742.